# Evolution of distorted rotating black holes. III. Initial data

Steven R. Brandt and Edward Seidel
*National Center for Supercomputing Applications, 605 East Springfield Avenue, Champaign, Illinois 61820 Department of Physics, University of Illinois at Urbana-Champaign, Urbana, Illinois 61801*
(Received 10 January 1996)

In this paper we study a new family of black hole initial data sets corresponding to distorted ''Kerr'' black holes with moderate rotation parameters, and distorted Schwarzschild black holes with even- and odd-parity radiation. These data sets build on the earlier rotating black holes of Bowen and York and the distorted Brill wave plus black hole data sets. We describe the construction of this large family of rotating black holes. We present a systematic study of important properties of these data sets, such as the size and shape of their apparent horizons, and the maximum amount of radiation that can leave the system during evolution. These data sets should be a very useful starting point for studying the evolution of highly dynamical black holes and can easily be extended to 3D. [S0556-2821(96)04114-8]

PACS number(s): 04.25.Dm, 95.30.Sf, 97.60.Lf

## I. INTRODUCTION

There is increasing interest in the study of black holes from both astrophysical and theoretical points of view. Coalescing black hole binaries are considered an important source of gravitational waves for the Laser Interferometric Gravitational Wave Observatory (LIGO) [1], VIRGO [2] and other gravitational wave observatories. At the same time, numerical studies of black holes are advancing to the point where highly distorted, axisymmetric black holes [3,4] and black hole collisions [5,6] can be simulated, extracting important physics such as the gravitational wave forms emitted and the dynamics and properties of the event and apparent horizons [7,8]. Recent progress has also been made in three dimensional (3D) [9] black hole spacetimes. These are some of the reasons it is important to develop a series of initial data sets to evolve.

However, black hole initial data sets are interesting in their own right, apart from evolutions. They are potentially useful for studying problems related to cosmic censorship, such as the Penrose inequality [10]. Furthermore, it is possible to study greater numbers of data sets with higher resolution than is practical to evolve numerically. This can lead to important observations of properties of apparent horizons and can help to identify particularly interesting spacetimes for evolution studies. Initial data sets of the type described in this paper can be used to analyze the most extreme types of distortion and may have bearing on the hoop conjecture [11,12]. The study of an apparent horizon in an initial data set may provide valuable insight into which spacetimes might have the most distorted event horizons.

Black hole initial data sets, based on the Einstein-Rosen bridge construction [13], have been developed over the last few decades. In the early 1960s a series of time symmetric, conformally flat wormhole data sets corresponding to two black holes were developed by Misner [14] and Brill and Lindquist [15]. At about the same time Brill developed an initial data set for gravitational wave spacetimes that involved specifying a free function in the conformal part of the three-metric that determined the distribution of the gravitational wave energy in the spacetime [16]. These time symmetric initial data sets were combined to produce the NCSA ''Brill wave plus black hole'' spacetimes, generalizing the single wormhole to a highly distorted black hole spacetime [10,17]. The evolution of these data sets has been very useful in understanding the dynamics of highly distorted black hole spacetimes, and also in preparing for studies of colliding black holes, as colliding holes form a highly distorted single hole immediately after the merging process. Rotating, stationary black hole data sets, which are not time-symmetric, were first discovered by Kerr [18] in 1963, and then a nonstationary form was discovered by Bowen and York [19]. The conformally flat Bowen and York construction for single black holes was then generalized to multiple conformally flat holes with angular momentum by a number of authors (for example, see [20]) leading to recently computed 3D data sets for two black holes with arbitrary spin and angular momentum [21].

In this paper we discuss a new family of distorted rotating black hole initial data sets, some of which were evolved and studied in Refs. [22–24]. Although the constructions we present here are axisymmetric, our approach is easily carried out in 3D. These data sets combine a number of the ideas discussed above, generalizing the Bowen and York construction by including a ''Brill wave'' so that highly distorted, rotating black holes with gravitational radiation can be studied. In addition to these new data sets to be described below, this family includes as special cases all previous single black hole data sets discussed above, including the Schwarzschild, Kerr, Bowen and York, and NCSA ''Brill wave plus black hole'' spacetimes.

As we have shown in Refs. [7,23,25], these data sets are interesting in their own right as dynamical black holes. These black holes radiate both polarizations of the gravitational wave field, and their horizon geometries can be so distorted they cannot be embedded in a flat Euclidean space. In future papers we will continue to explore their dynamics in detail. Moreover, just as in the nonrotating case, these data sets can be used to understand the late time behavior of coalescing, multiple black hole systems, as highly distorted ''Kerr'' black holes will be formed in the process. These data sets can be thought of as representing initial conditions

 

for the late stages of that process, and should prove to be a valuable system for studying it without having to evolve the orbits leading up to the merger.

The paper is organized as follows: In Sec. II we detail the mathematical construction of the data sets and discuss some of their properties, such as their masses, for several subclasses of the spacetimes. Then in Sec. III we discuss a series of tools we have developed to study the initial data sets, such as the apparent horizons and their intrinsic geometry. In Sec. IV we survey many initial data sets, describe their features, and discuss application of the hoop conjecture and Penrose inequality. Finally in Sec. V we summarize the results.

## II. CONSTRUCTING DISTORTED, ROTATING BLACK HOLES

### A. Initial data

In this section we provide details of the construction of this new family of distorted, rotating black hole data sets. Some details were provided in Ref. [22], but as this paper focuses exclusively on the initial value problem we present a more comprehensive treatment here. To motivate the problem, consider first the Kerr metric, written in Boyer-Lindquist form [26]:

$$g^{(K)}_{\mu\nu}=\begin{pmatrix} g^{(K)}_{tt} & 0 & 0 & g^{(K)}_{t\phi} \\ 0 & g^{(K)}_{rr} & 0 & 0 \\ 0 & 0 & g^{(K)}_{\theta\theta} & 0 \\ g^{(K)}_{t\phi} & 0 & 0 & g^{(K)}_{\phi\phi} \end{pmatrix},$$

$$\begin{aligned} g^{(K)}_{rr}&=\rho^2/\Delta, \\ g^{(K)}_{\theta\theta}&=\rho^2, \\ g^{(K)}_{tt}&=(a^2\sin^2\theta-\Delta)/\rho^2, \\ g^{(K)}_{t\phi}&=-2amr\sin^2\theta/\rho^2, \\ g^{(K)}_{\phi\phi}&=[(r^2+a^2)^2-\Delta a^2\sin^2\theta]\sin^2\theta/\rho^2, \\ \Delta&=r^2-2mr+a^2, \\ \rho^2&=r^2+a^2\cos^2\theta, \end{aligned} \tag{1}$$

where $m$ is the mass of the Kerr black hole, $a$ is the angular momentum parameter, and a superscript $(K)$ denotes the Kerr spacetime.

We would like to put this in a form that is free of coordinate singularities, and that has properties similar to the form used in the nonrotating black hole studies [4,17,27]. Generalizing the transformation used in Ref. [4,17,27] we define a new radial coordinate $\eta$ through

$$r=r_+\cosh^2(\eta/2)-r_-\sinh^2(\eta/2), \tag{2a}$$

$$r_\pm=m\pm\sqrt{m^2-a^2}. \tag{2b}$$

With this transformation the spatial part of the Kerr metric can be written as

$$dl^2=\Psi_0^4[e^{-2q_0}(d\eta^2+d\theta^2)+\sin^2\theta d\phi^2], \tag{3}$$

where

$$\Psi_0^4=g^{(K)}_{\phi\phi}/\sin^2\theta, \tag{4a}$$

$$\Psi_0^4 e^{-2q_0}=g^{(K)}_{rr}\left(\frac{dr}{d\eta}\right)^2=g^{(K)}_{\theta\theta}. \tag{4b}$$

Thus we see that our coordinate transformation (2b) has resulted in a ''quasi-isotropic gauge'' [28] for the Kerr spacetime. Notice also that if $a=0$ then $q_0=0$ and we recover the Schwarzschild three-metric. This metric is now in the form used in the previous NCSA black hole studies [3,4,17,29], although here the functions $q_0$ and $\Psi_0$ are determined by the Kerr spacetime.

One may check that the three-metric defined by Eq. (3) is invariant under the transformation $\eta\rightarrow-\eta$, i.e., there is an isometry operation across the throat of an Einstein-Rosen bridge located at $\eta=0$, just as in the Schwarzschild spacetime [30]. This construction has two geometrically identical sheets connected smoothly at the throat, located at $\eta=0$. In terms of the more familiar radial coordinates, this condition can be expressed as

$$\overline{r}\rightarrow(m^2-a^2)/(4\overline{r}), \tag{5}$$

where $\overline{r}$ is a generalization of the Schwarzschild isotropic radius, defined as

$$\overline{r}=\frac{\sqrt{m^2-a^2}}{2}e^{\eta}. \tag{6a}$$

$\overline{r}$ is related to the usual Boyer-Lindquist radial coordinate via

$$r=\overline{r}\left(1+\frac{m+a}{2\overline{r}}\right)\left(1+\frac{m-a}{2\overline{r}}\right). \tag{6b}$$

Note that in the Kerr spacetime the horizon, located at $r=m+\sqrt{m^2-a^2}$, is at $\overline{r}=\sqrt{m^2-a^2}/2$ in the $\overline{r}$ coordinates, or at $\eta=0$, just as in previous studies of the Schwarzschild spacetime [30]. The isometry condition $\eta\rightarrow-\eta$ will be used in the construction of more general initial data sets to be described below, and is also imposed during the evolution as well [23].

The three-metric, however, comprises only half of our initial data. The extrinsic curvature on the initial slice is required as well, and for the Kerr spacetime it is given by the equations

$$\hat{K}_{\eta\phi}=am[2r^2(r^2+a^2)+\rho^2(r^2-a^2)]\sin^2\theta\rho^{-4}, \tag{7a}$$

$$\hat{K}_{\theta\phi}=-2a^3mr\Delta^{1/2}\cos\theta\sin^3\theta\rho^{-4}, \tag{7b}$$

where we note that $K_{ij}=\Psi_0^{-2}\hat{K}_{ij}$, and all extrinsic curvature components excepting the two listed are zero. One can show that this metric and extrinsic curvature satisfy both the Hamiltonian constraint

$$R+K^2-K^{ij}K_{ij}=0 \tag{8}$$

and the three-momentum constraints

$$\nabla_i(K^{ij}-\gamma^{ij}K)=0, \tag{9}$$

as they must.

Finally we must specify the lapse and shift to complete the system for evolution. The choices that make the stationary nature of this Kerr spacetime explicit are

$$\frac{1}{\alpha^2}=1+2\,mr\left(\frac{r^2+a^2}{\Delta\rho^2}\right) \tag{10}$$

and

$$\beta^{\phi}=\frac{-2amr}{(r^2+a^2)^2-a^2\Delta\sin^2\theta}. \tag{11}$$

We have now written the Kerr spacetime in 3+1 form, in a coordinate system like that used to evolve the nonrotating distorted black holes in previous work. This is a stationary spacetime, and it can be evolved using a dynamic slicing condition just as the Schwarzschild spacetime has been evolved using maximal and other slicing conditions. But just as in the case of Schwarzschild, we can distort this rotating black hole with a gravitational (''Brill'') wave and study its response.

We accomplish this by adding a free function $q(\eta,\theta)$ to the conformal three-metric in Eq. (3), just as in Ref. [17]. Then the conformal factor $\Psi_0$, which is a solution only for the stationary Kerr spacetime, will no longer satisfy the Hamiltonian constraint (8). Instead we must solve this constraint equation for the general conformal factor $\Psi$ as we discuss below. This generalization results in a three-metric with the form

$$dl^2=\Psi^4[e^{2(q-q_0)}(d\eta^2+d\theta^2)+\sin^2\theta d\phi^2]. \tag{12}$$

Apart from the function $q_0$ this is the same three-metric used for the nonrotating, distorted black hole spacetime. This illustrates the fact that unlike the Schwarzschild spacetime the undistorted Kerr spacetime is *not* conformally flat ($\hat{R}\neq 0$, where $\hat{R}$ is the scalar curvature of the conformal part of the three-metric). We may, in fact, make the spacetime conformally flat by adding a ''Brill wave'' [19] specified by $q=q_0$. This distorts the Kerr black hole, which breaks the stationary nature of the spacetime. As we will show below, appropriate choices of this function $q$ (along with appropriate solutions to the momentum constraint for the extrinsic curvature terms) can lead also to Schwarzschild, the NCSA distorted nonrotating black hole (as in Ref. [17]), the Bowen and York rotating black hole [19], or a distorted Bowen and York black hole.

The function $q$, representing the Brill wave, can be chosen somewhat arbitrarily, subject to symmetry conditions on the throat, axis and equator, and falloff conditions at large radii [17,22]. The function $q$ will be chosen to have an inversion symmetric (i.e., symmetric under $\eta\rightarrow-\eta$) Gaussian part given by

$$q=\sin^n\theta q_G, \tag{13a}$$

$$q_G=Q_0(e^{-s_+}+e^{-s_-}), \tag{13b}$$

$$s_{\pm}=(\eta\pm\eta_0)^2/\sigma^2. \tag{13c}$$

This form of the Brill wave will be characterized by several parameters: $Q_0$ (its amplitude), $\sigma$ (its width), $\eta_0$ (its coordinate location), and $n$, specifying its angular dependence, which must be positive and even. We note that Eqs. (13) simply provide a convenient way to parametrize the initial data sets, and to allow us to easily adjust the ''Brill wave'' part of the initial data. Many other devices are possible. To narrow the field of study, in this paper we restrict ourselves to sets characterized by $n=2$, and $\eta_0=0$ for all data sets, and will commonly use $\sigma=1.5$

With this form of the Brill wave function $q$, a number of black hole data sets can be constructed. As discussed above, given the appropriate extrinsic curvature choice, the stationary Kerr solution results if $q=0$. For other choices the Bowen and York form results if $q=q_0$; a *distorted* Bowen and York spacetime can be made by setting $q=\sin^n\theta q_G+q_0$; and a distorted Kerr spacetime can be made by setting $q=\sin^n\theta q_G$. Furthermore, for spacetimes without angular momentum this metric form contains both the NCSA Brill wave plus black hole spacetimes and, as we will see below, a new black hole spacetime corresponding to odd-parity distortions of the Schwarzschild spacetime.

As a consequence of this generalization of the metric, we must now solve both the Hamiltonian and momentum constraints. The Hamiltonian constraint equation (8) can be expanded in coordinate form to yield

$$\begin{aligned}\frac{\partial^2\Psi}{\partial\eta^2}+\frac{\partial^2\Psi}{\partial\theta^2}+\frac{\partial\Psi}{\partial\theta}\cot\theta-\frac{\Psi}{4}&\\ =-\frac{\Psi}{4}\left(\frac{\partial^2}{\partial\eta^2}(q-q_0)+\frac{\partial^2}{\partial\theta^2}(q-q_0)\right)&\\ -\frac{\Psi^{-7}}{4}(\hat{H}_E^2\sin^2\theta+\hat{H}_F^2),&\end{aligned} \tag{14}$$

where we have assumed the initial slice is maximal, i.e., tr K=0. There are in principle three momentum constraints to be satisfied by the extrinsic curvature components. However, in our spacetimes we require a ''time-rotation'' symmetry about the initial slice, or invariance of the metric under $(t,\phi)\rightarrow(-t,-\phi)$. Writing the extrinsic curvature tensor as

$$K_{ij}=\Psi^{-2}\hat{H}_{ij}=\Psi^{-2}\begin{pmatrix}\hat{H}_A & \hat{H}_C & \hat{H}_E\sin^2\theta\\ \hat{H}_C & \hat{H}_B & \hat{H}_F\sin\theta\\ \hat{H}_E\sin^2\theta & \hat{H}_F\sin\theta & \hat{H}_D\sin^2\theta\end{pmatrix}, \tag{15}$$

this time-rotation symmetry requires that

$$\hat{H}_A=\hat{H}_B=\hat{H}_C=\hat{H}_D=0, \tag{16}$$

leaving only $\hat{H}_E$ and $\hat{H}_F$ to be determined. This also automatically makes the initial slice maximal.

Under these conditions the only nontrivial component of the momentum constraints is the $\phi$ component:

$$\partial_\eta \hat{H}_E \sin^3\theta + \partial_\theta(\hat{H}_F \sin^2\theta) = 0. \tag{17}$$

Note that this equation is independent of the functions $q$ and $q_0$. This enables us to choose the solutions to these equations independently of our choice of metric perturbation.

At this point we may regard Eqs. (12)–(17) as defining the problem we wish to solve. The boundary conditions for these equations, which are extensions of those used in Ref. [17], may be summarized as follows.

*Isometry conditions*. Across the throat of the black hole, labeled by $\eta=0$, we can demand a condition that the spacetime has the same geometry as $\eta \to -\eta$. We can require this not only for the initial data, but also throughout the evolution of the spacetime. This condition may be stated in one of two ways (in axisymmetry) to allow for different slicing conditions. Each choice must result in a symmetric $K_{\eta\phi}$ and an antisymmetric $K_{\eta\theta}$ to be consistent with the Kerr solution. Thus, the form of the isometry condition must be different for the symmetric and antisymmetric lapse spacetimes: $\eta \to -\eta$ for the former, $(\eta,\phi) \to (-\eta,-\phi)$ for the latter.

If a lapse that is antisymmetric across the throat is desired, the metric elements with a single $\eta$ index are antisymmetric across the throat, while those with zero or two indices are symmetric. The extrinsic curvature components have the opposite symmetry of their corresponding metric elements. The shift $\beta^\eta$ is antisymmetric across the throat, while all other shifts are symmetric.

If a symmetric lapse is desired, the metric elements with a single $\eta$ index or single $\phi$ index (but not both) will be antisymmetric at the throat and all others will be symmetric. Extrinsic curvature components will have the same symmetries as their corresponding metric elements. The $\beta^\eta$ and $\beta^\phi$ shifts will be antisymmetric, and the $\beta^\theta$ shift will be symmetric. With these symmetries enforced, the initial data and all subsequent time slices will be isometric across the throat. One can verify that all Einstein equations respect these symmetries during the evolution if they are satisfied initially.

*Symmetry axis*. All metric elements, extrinsic curvature components, and shift components with a single $\theta$ index are antisymmetric across the axis. The remainder are symmetric.

*Equatorial plane*. At the equator there are two possible symmetries, the Kerr symmetry and the ''cosmic screw'' symmetry (see Sec. II A 4 below). For the Kerr symmetry, $\theta \to \pi-\theta$, all metric components, extrinsic curvature components or shifts with a single $\theta$ index are antisymmetric. The remainder are symmetric. For the cosmic-screw type boundary conditions the symmetry at the equator is $(\theta,\phi) \to (\pi-\theta,-\phi)$ and those metric elements, extrinsic curvature components, or shift components that contain one $\theta$ or one $\phi$ index (but not both) are antisymmetric. The remainder are symmetric.

*Outer boundary*. At the outer boundary a Robin condition is used for $\Psi$. This condition gives the correct asymptotic behavior in the conformal factor to order $r^{-2}$. For the metric given in the form (12) $\Psi$ has the form $\Psi = e^{\eta/2} + (m/2)e^{-\eta/2} + \cdots$ and therefore obeys the differential equation $\Psi + 2\partial_\eta \Psi = 2e^{\eta/2}$. The conformal factor is always symmetric at the throat, axis, and equator.

With this description of the problem and boundary conditions, we summarize a number of families of rotating black hole solutions that are possible in this formulation.

#### *1. Kerr and distorted Kerr*

As shown above, Eqs. (12)–(17), together with the boundary conditions, are satisfied by the stationary Kerr spacetime with the transformations (2)–(7). In Eq. (12), this spacetime corresponds to $q=0$, but as we have mentioned above, we may add a Brill wave function $q=\sin^n\theta q_G$ to distort the Kerr spacetime. From the standard Arnowitt-Deser-Misner (ADM) expressions for the mass and angular momentum of the spacetime [31] we have

$$M_{\rm ADM} = -\frac{1}{2\pi}\oint_S \nabla_a(\Psi e^{-\eta/2})dS^a, \tag{18a}$$

$$P_a = \frac{1}{8\pi}\oint_S (H^b_a - \gamma^b_a H)dS_b, \tag{18b}$$

or, in terms of the variables defined in this paper,

$$M_{\rm ADM} = \int_0^\pi e^{\eta/2}(-\partial_\eta \Psi + \Psi/2)\sin\theta d\theta, \tag{19a}$$

$$J = P_\phi = \frac{1}{4}\int_0^\pi \Psi^6 H_E \sin^3\theta d\theta. \tag{19b}$$

If one evaluates these expressions for the undistorted Kerr spacetime, $(q=0)$, one recovers the expected results $M_{\rm ADM}=m$ (which should be evaluated at $\eta=\infty$) and $J=am$ (which may be evaluated at any radius in axisymmetry). In practice, we evaluate $m$ at the outer edge of our grid, and $J$ is simply an input parameter. We have evaluated and verified $J$ at various radii, as reported in previous work [22].

#### *2. Distorted Bowen and York*

Perhaps the simplest nontrivial choice of solution for the momentum constraint is given by the Bowen and York [19] solution

$$\hat{H}_E = 3J, \tag{20a}$$

$$\hat{H}_F = 0, \tag{20b}$$

where $J$ is the total angular momentum of the spacetime. This solution clearly satisfies the momentum constraint. In the language of this paper, the original Bowen and York solution has a Brill wave function determined by

$$q = q_0; \tag{21}$$

i.e., it is conformally flat, but we may distort it by setting

$$q = q_0 + \sin^n\theta q_G. \tag{22}$$

This is the solution we often use in constructing distorted rotating black hole spacetimes, and a number of them have

been evolved and discussed in Ref. [23]. It is somewhat simpler to construct than the distorted Kerr because we can choose our total angular momentum and distortion parameters without needing to know the ratio $J/m^2$ (an additional value that we would need to initialize the Kerr momentum solution). Knowing this parameter would require us to know the value $m$, and we will not know that parameter until after we solve the Hamiltonian constraint. It is possible, in principle, to iterate between guesses for the parameter $J/m^2$ and solutions for the Hamiltonian constraint until arriving at a correctly initialized Kerr momentum solution.

We noted above that the Kerr solution is not conformally flat, while the Bowen and York solution is conformally flat. Therefore one can consider adding a Brill wave to the Kerr solution, making it a conformally flat Bowen and York solution. One can study the form of the wave functions $q$ and $q_0$ to understand what sort of Brill wave is required to ''flatten'' the Kerr solution. By equating the series expansions of $q_0$ and our Brill wave function [cf. Eq. (4b)],

$$q_{\rm approx}=a_1\sin^2\theta e^{-\eta^2/\sigma_1^2}+a_2\sin^4\theta e^{-\eta^2/\sigma_2^2}, \tag{23}$$

to second order in $\eta$ and $\theta$, one obtains relationships between the wave shape parameters $a_1$, $a_2$, $\sigma_1$, and $\sigma_2$ and the Kerr parameters $a$ and $m$. It turns out that for $a/m<0.9$ we find that the $\sin^2\theta$ term dominates the $\sin^4\theta$ term, and $\sigma_1$ varies in value from 1.26 to 1.7 for rotation parameters $0.01\leqslant a/m\leqslant 0.8$. Furthermore the amplitude $a_1$ varies smoothly from zero to about 0.38 for all rotation parameters $0\leqslant a/m\leqslant 1$. We conclude that the Bowen and York distortion is similar to a low amplitude $n=2$, $\sigma=1.5$ Brill wave distortion on a Kerr black hole, which is quite similar in shape and size to the distorted, non-rotating black holes evolved previously [3].

To get a feel for the difference between the $q_0$ function and its approximation, $q_{\rm approx}$, we calculated the ADM value of $a/M_{\rm ADM}$ as we would for the Kerr spacetime, except that we used $q_{\rm approx}$ instead of $q_0$ in the metric. We found that the error in $a/M_{\rm ADM}$ was less than 1%, even for $a/m=0.9$.

#### *3. Odd-parity distorted Schwarzschild*

Odd-parity gravitational modes, as defined by Regge and Wheeler [32], are metric perturbations with parity $(-1)^{\ell+1}$ where $\ell$ is the angular index of the tensor spherical harmonic describing the wave. These modes, in axisymmetry, are formed only from perturbations in $g_{r\phi}$ and $g_{\theta\phi}$. The evolution of these modes does not couple linearly to the even-parity modes, and if there is no odd-parity disturbance on the initial slice of the spacetime these modes are never excited even when the full nonlinear equations are used.

We can create odd-parity distorted nonrotating spacetimes simply by finding solutions to the momentum constraint equation (17) which drive the evolution of $g_{\theta\phi}$, which satisfy the boundary conditions, and yield $J=0$ when the integral given in Eq. (19b) is performed.

As a framework for momentum solutions, we consider the simple class defined by

$$\hat{H}_E=f_1(\theta)+f_2(\eta)[4\cos\theta f_3(\theta)+\sin\theta\partial_\theta f_3(\theta)], \tag{24a}$$

$$\hat{H}_F=-\partial_\eta f_2(\eta)\sin^2\theta f_3(\theta). \tag{24b}$$

This solves the momentum constraint where $f_1$, $f_2$, and $f_3$ are arbitrary functions which satisfy the symmetries

$$f_1(\theta)=f_1(-\theta)=f_1(\pi-\theta), \tag{25a}$$

$$f_3(\theta)=-f_3(-\theta)=-f_3(\pi-\theta), \tag{25b}$$

$$f_2(\eta)=f_2(-\eta), \tag{25c}$$

$$\lim_{\eta\to\infty} f_2(\eta)=0. \tag{25d}$$

The Kerr solution is not a member of this class, but the Bowen and York solution does fit within it ($f_1=3J$, $f_2=f_3=0$).

Note that any spacetime with $f_1=0$ will have zero angular momentum, as $\hat{H}_E$ falls off for large values of the radial coordinate $\eta$, and furthermore the angular part of the integral in Eq. (19b) is identically zero by construction. We require $f_2$ to go to zero only so that we can make the spacetime asymptotically Kerr.

We now turn to a solution that has no net angular momentum, but one that is not time symmetric about the initial slice. This solution corresponds to a ''Schwarzschild'' black hole with both even- and odd-parity distortions. This generalizes the NCSA Brill wave plus black hole spacetimes [29], which allowed only even-parity distortions.

For this we choose the extrinsic curvature components such that $f_1=0$, $f_2=q_G'$, and $f_3=\cos\theta\sin^{n'-3}\theta$. In order to obey symmetry and regularity conditions, $n'$ must be odd and have a value of at least three. (This was arranged to be suggestive of a radiation $\ell$ mode. Using $n=3$ gives almost pure $\ell=3$, while using $n=5$ gives almost a pure $\ell=5$ component [23].)

As this data set contains the odd-parity polarization of the gravitational wave field, but no angular momentum, it is simpler to evolve than than the rotating black holes described above, but has richer physical content than the standard Brill wave plus black hole data sets. A few of these data sets have been evolved and discussed in Ref. [23], where both even- and odd-parity waveforms were extracted.

#### *4. Cosmic screws*

There is another solution related to the odd-parity distorted Schwarzschild data set discussed above. While that data set has equatorial plane symmetry, we can alternatively construct a solution that has something like an opposite sense of rotation below the equatorial plane. As discussed above, this symmetry is $(\theta,\phi)\to(\pi-\theta,-\phi)$, thus requiring $\hat{H}_E$ to be antisymmetric and $\hat{H}_F$ to be symmetric across the equator.

Axisymmetric data sets describing the collision of two counter-rotating black holes have been dubbed ''cosmic screws.'' As our data sets contain only one black hole, it can be considered to represent a later stage of evolution of cosmic screws, where the holes have already merged. Such data sets should be useful in studying the late time behavior of colliding spinning black holes, and will be evolved in a future paper. The formalism of the previous section carries over, but now the symmetry conditions on the equator are reversed: $f_1(\theta)=-f_1(\pi-\theta)$ and $f_3(\theta)=f_3(\pi-\theta)$.

With these considerations in mind, we see that $f_1=3J\cos\theta$, and $f_2=f_3=0$ is suggestive of a cosmic screw spacetime (in this case we do not claim that $J$ is an angular momentum, but use this notation because it is suggestive of the angular momentum of one of the colliding black holes in a cosmic-screw spacetime).

We can also choose $f_1=0$, $f_2=q'_G$, and $f_3=\sin^{n'-2}\theta$ which is similar to our odd-parity distortion of Schwarzschild except that the equatorial boundary conditions are like those of the cosmic screw. Here $n'$ should be even and have a value of at least 2 in order to obey symmetry and regularity requirements.

### B. Numerical techniques

To solve the Hamiltonian constraint equation we use a Newton-Raphson iteration procedure. The conformal factor in the constraint equation is linearized about a trial function. The initial trial function, $\Psi_0$, is usually chosen to be $2\cosh(\eta/2)$, because that is the solution for a spherical black hole with mass $M=2$. At a given iteration $i$ we assume the solution has the form $\Psi=\Psi_i+\delta\Psi$, where $\delta\Psi$ is a small correction function. We then evaluate the residual $\epsilon_i$ of this guess for $\Psi_i$,

$$\epsilon_i=\triangle\Psi_i+\frac{\Psi_i}{4}(\partial_\eta^2(q-q_0)+\partial_\theta^2(q-q_0))-\frac{\Psi_i^{-7}}{4}(\hat{H}_E^2\sin^2\theta+\hat{H}_F^2), \tag{26a}$$

and use it as a source term for the correction function $\delta\Psi$:

$$\triangle\delta\Psi+\frac{\delta\Psi}{4}(\partial_\eta^2(q-q_0)+\partial_\theta^2(q-q_0))+7\,\delta\Psi\frac{\Psi_i^{-8}}{4}(\hat{H}_E^2\sin^2\theta+\hat{H}_F^2)=-\epsilon_i\,. \tag{26b}$$

Equation (26a) is used merely to evaluate $\epsilon_i$, but Eq. (26b) is solved with a numerical elliptic solver for $\delta\Psi$. The boundary conditions on the grid are given as follows: $\delta\Psi$ is symmetric across the throat, the axis, and the equator. At the outer boundary we use the Robin condition, $\partial_\eta\delta\Psi=-\frac{1}{2}\delta\Psi$. Typically we use $\epsilon=10^{-7}$ as our stopping criterion.

Once $\delta\Psi$ is obtained, we try again, with $\Psi_{i+1}=\Psi_i+\delta\Psi$. We repeat this procedure until a solution to Eq. (14) with appropriately small error (maximum value of $\epsilon_i$ on the grid) is achieved [20].

Some of the data sets considered in this paper use Brill waves that are very wide. Because of this, one may worry whether the outer boundary of the grid is sufficiently large to get an appropriate asymptotic behavior for the Hamiltonian constraint. To determine whether the position of $\eta_{\max}$ is valid, we measure the quantity

$$\xi=\partial_\eta\ln|\Psi-e^{\eta/2}| \tag{27}$$

which should approach $-1/2$ in a spacetime that asymptotically approaches the Kerr spacetime. We adopt the criterion that $\xi$ must be equal to this value to within 0.1%. If it is not, we regard our choice for value of $\eta_{\max}$, the outer boundary of our grid, to be too small and adjust accordingly.

### C. Limits on the magnitude of Brill wave amplitudes

Cantor and Brill [33] showed that for a certain class of spacetimes there are limits on the value of the amplitude of the Brill wave in a spacetime with topology $R^3$. Their basic technique can be applied to these rotating black hole spacetimes, which have topology $R\times S^2$. We present a simplified version of this analysis.

The strategy is to derive an inequality that contains an arbitrary function $f$, but does not explicitly contain the conformal factor $\Psi$, and which requires asymptotic flatness of the spacetime as one of its conditions for validity. We use the freedom in $f$ to locate Brill wave parameter spaces which fail to satisfy the inequality. When the inequality fails, it is then clear that the assumption of asymptotic flatness has been violated, and the value of the input Brill wave parameters which specify it are outside our domain of interest.

For this section, we define the metric as

$$ds^2=\tilde{\Psi}^4e^{2\eta}[e^{2(q-q_0)}(d\eta^2+d\theta^2)+\sin^2\theta d\phi^2]. \tag{28}$$

Brill started by considering the volume integral

$$\int\hat{\nabla}f\cdot\hat{\nabla}f\,dV, \tag{29}$$

where $f=u\tilde{\Psi}$, and where $u$ or $f$ is an arbitrarily chosen function. We can expand the above integral for $f$ in terms of $u$ and $\tilde{\Psi}$:

$$\hat{\nabla}\cdot(u^2\tilde{\Psi}\hat{\nabla}\tilde{\Psi})-u^2\tilde{\Psi}\,\hat{\triangle}\,\tilde{\Psi}=2u\tilde{\Psi}\hat{\nabla}u\cdot\hat{\nabla}\tilde{\Psi}+u^2\hat{\nabla}\tilde{\Psi}\cdot\hat{\nabla}\tilde{\Psi}. \tag{30}$$

We have now obtained both a surface and a volume piece for the integral. Because we want a final equation which does not include $\tilde{\Psi}$, we discard the terms under the integral which still contain it explicitly after our transformation. Since these terms are manifestly positive, the remainder must be less than our original integral. We now have an inequality. Next we require that $\tilde{\Psi}$ not vanish (this is only necessary if we have nonzero extrinsic curvature), is finite, and that $\hat{\nabla}u$ go to zero faster than $r^{-3/2}$.

To evaluate the surface terms we make use of the asymptotic properties of $\tilde{\Psi}$, namely that $\tilde{\Psi}=1+m/2r+O(r^{-2})$ at large radii. The surface term is

$$\oint u^2\tilde{\Psi}\hat{\nabla}\tilde{\Psi}\cdot dS. \tag{31}$$

This last expression will be $-2\pi$ times the ADM mass of the system if we choose $u\to\Psi^{-1}$ at $\eta\to\infty$. If we choose $u\to0$ as $\eta\to\infty$ then the integral will not evaluate to the ADM mass (in fact it will obtain zero). When we perform this surface integral at the throat of our spacetime we exploit the isometry

$$\partial_\eta(\tilde{\Psi}e^{\eta/2})=0, \tag{32}$$

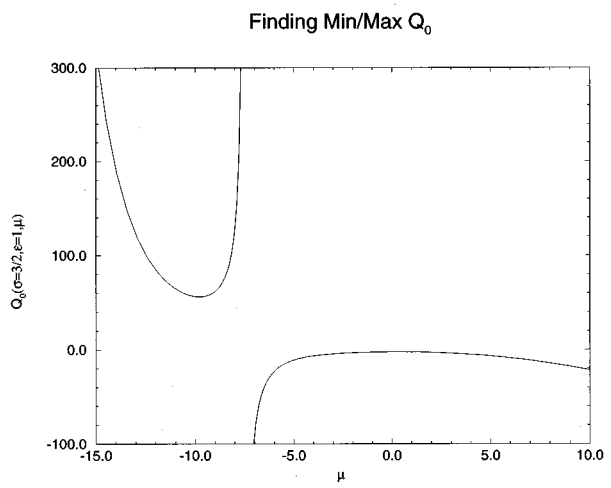


FIG. 1. We plot the range of the Brill wave amplitude function $Q_0$ which are inconsistent with asymptotically flat solutions of the Hamiltonian constraint for a given ''trial function'' (see text). In this example plot, the values outside the range $-2.317<Q_0<56.24$ are excluded.

to obtain the final form for our inequality

$$2\pi f^2_{\eta=\infty} M_{\rm ADM} + \int \left( \hat{\nabla} f \cdot \hat{\nabla} f + \frac{1}{8} f^2 \hat{R} \right) dV > \pi \int_0^\pi f^2_{\eta=0} \sin\theta d\theta. \quad (33)$$

where we have assumed that $f$ is independent of $\theta$ at large $\eta$. This inequality can only fail if our assumptions about the form of $\tilde{\Psi}$ are incorrect. Therefore, when it does fail, we can conclude that an asymptotically flat metric cannot be formed by the given Brill wave parameters.

We explored the regime where $q=\sin^n\theta q_G+q_0=2Q_0\sin^2\theta e^{-\eta^2/\sigma^2}$ and found two forms for $f$ which provided us with good bounds on the integral. These forms are

$$f=\exp(-\epsilon\eta^2-\mu\eta/2) \quad (34)$$

and

$$f=\cos^4\theta\exp(-\epsilon\eta^2-\mu\eta/2). \quad (35)$$

Replacing the inequality with an equality in Eq. (33), performing the integral, and then solving for $Q_0$ provides us with a function $Q_0(\mu,\epsilon,\sigma)$ whose range supplies the forbidden amplitude values $Q_0$ and whose domain is $\epsilon>0$, $\sigma>0$, and $\mu$ is a real number.

The functions $Q_0(\mu,\epsilon,\sigma)$ that we obtained were able to provide both an upper and a lower bound for the allowed values of the input parameter $Q_0$ because they trace out a function similar to an hyperbola in $\mu$ space for given values of $\sigma$ and $\epsilon$. The behavior of one function is illustrated in Fig. 1. In this figure we see two distinct extrema. One extremum is a greatest possible negative value for $Q_0$ and provides us with a lower bound for this parameter. The other is a minimum in the possible positive values for $Q_0$ and this provides us with a maximum value for $Q_0$.

TABLE I. Upper limits on $Q_0$. The parameters $\epsilon$, $\mu$, and $n$ are arbitrary parameters and were chosen in an attempt to find the smallest upper bound for the allowed values of $Q_0$, the wave amplitude, as a function of the wave width $\sigma$.

| $\sigma$ | $\epsilon$ | $\mu$ | $n$ | $Q_0$ |
|---|---|---|---|---|
| 0.25 | 1.726 | −2.928 | 0 | 3.283 |
| 0.50 | 1.078 | −3.186 | 0 | 5.122 |
| 0.75 | 0.8455 | −3.64 | 0 | 7.516 |
| 1.00 | 0.7042 | −4.037 | 0 | 10.74 |
| 1.25 | 0.6171 | 1.096 | 4 | 11.97 |
| 1.50 | 0.5580 | 1.097 | 4 | 10.99 |
| 1.75 | 0.5049 | 1.087 | 4 | 10.35 |
| 2.00 | 0.4587 | 1.076 | 4 | 9.914 |
| 3.00 | 0.3300 | 1.046 | 4 | 8.993 |
| 100.0 | 0.0100 | 1.014 | 4 | 7.6113 |

In Table I we have give the strictest upper bound for the function $Q_0$ that we were able to find using the above inequality, Eq. (33), and trial functions, Eqs. (34) and (35). These bounds, together with the parameters $\mu$ and $\epsilon$ which were chosen to minimize them, are given in the table.

If one explores the $\mu=1$ form of this distortion and takes the limits $\sigma\to\infty$ and $\epsilon\to0$ in that order one arrives at the amplitude $Q_0=7.577$. Thus, it seems that while there are more strict limits on larger width waves in general, there is no reason to suspect that any width is too large.

In Table II we have the strictest lower bound for the function $Q_0$ that we were able to find using the methods of this section.

It is interesting to note, however, that the pure Bowen and York spacetime (which is parametrized by $J$, not $Q_0$ and can be regarded as a distortion of the Kerr spacetime) can be specified apparently without limit. This is consistent with the calculation done here, because the conformal Ricci scalar vanishes for conformally flat spacetimes such as the Bowen and York spacetime. This assures us that the inequality given in Eq. (33) is trivially satisfied. Numerical evaluations of the Bowen and York black hole (see [34]) seem to get asymptotically closer to the extremal Kerr spacetime as $J$ is increased, i.e., $J/m^2=a/m$ gets ever closer to unity confirming this observation.

TABLE II. Lower limits on $Q_0$. The parameters $\epsilon$, $\mu$, and $n$ are arbitrary parameters and were chosen in an attempt to find the greatest lower bound for the allowed values of the wave amplitude $Q_0$, and the wave width $\sigma$.

| $\sigma$ | $\epsilon$ | $\mu$ | $n$ | $Q_0$ |
|---|---|---|---|---|
| 0.25 | 0.0025 | 2.81 | 0 | −1.261 |
| 0.50 | 0.0025 | 2.31 | 0 | −1.437 |
| 0.75 | 0.0558 | 1.94 | 0 | −1.486 |
| 1.00 | 0.1053 | 1.62 | 0 | −1.456 |
| 1.25 | 0.1133 | 1.44 | 0 | −1.404 |
| 1.50 | 0.1081 | 1.33 | 0 | −1.351 |
| 1.75 | 0.1001 | 1.26 | 0 | −1.303 |
| 2.00 | 0.0921 | 1.21 | 0 | −1.260 |
| 100.0 | 0.0487 | 1.00 | 0 | −0.765 |

We note also that we can use Eq. (33) to obtain a lower bound on the ADM mass for numerically derived data sets. Using $f=1$ we obtain

$$M_{\rm ADM} > 1 + \frac{1}{4}\int_0^{\pi} (q - q_0)\sin\theta d\theta, \tag{36}$$

where the integral is evaluated on the throat. We calculate this after computing $\Psi$ on the initial slice to determine whether the ADM mass of the spacetime is consistent with asymptotic flatness.

## III. APPARENT HORIZONS

### A. The numerical method

We will use the same method for finding the AH (apparent horizon) as described in previous work [10,23], where surfaces that satisfy the trapped surface equation

$$D_i s^i + K_{ij} s^i s^j - K = 0 \tag{37}$$

are sought. In the above, $s^i$ is an outward pointing unit normal vector which defines the surface. For initial data sets of the type considered in this paper, the terms containing the extrinsic curvature drop out, and therefore finding the apparent horizon reduces to finding an extremal surface. We will, however, be using a different strategy for searching than we used when we were evolving our spacetimes [22,23]. For extremely distorted data sets we found that multiple trapped surfaces may exist, and it is important to find the *outermost* surface. Therefore, we use a ''brute force'' approach and repeatedly call the solver, using many constant radial zones covering the inner portion of the grid as an initial guess. After the horizon finder has finished executing for each initial guess, the solution with the largest radial coordinate position that satisfied the tolerance of the solver was determined to be the apparent horizon.

This strategy relies on our previous experience, which has shown us that even horizons with highly distorted geometry are nearly spherical in coordinate space, in our choice of coordinates. Moreover, we know, from Gibbons [35], that our apparent horizon must have the topology of a two-sphere. As in previous papers [23,25], we will study the intrinsic geometry of the black hole horizon as a measure of its distortion.

### B. Measures of the horizon

There are a number of geometric quantities that can be used to measure the apparent horizon that provide insight to the physical characteristics of the black hole. Examples are its shape, area, and local curvature. One straightforward measure of a black hole's shape in axisymmetry is the ratio of its polar circumference, $C_p$, to its equatorial circumference, $C_e$. This ratio has been used previously, but we point out that it has an inadequacy. If used to study the surface of an event horizon, this number may be infinitely large for some configurations; one need merely consider the case where two equal mass black holes are colliding and are just touching so that $C_e$ vanishes. Although we do not expect this problem to affect the apparent horizon, however, we would like to use the same measure of oblateness for both apparent and event horizons, one which better captures the intuitive concept of oblateness. One such measure is $C_p/C_A$, where $C_A = 2\pi(2\sqrt{A/16\pi})$ is the ''areal circumference.'' Note that the quantity $C_p/C_A$ tends to be much smaller than $C_p/C_e$. For the case of a $\sigma=3.5$, $Q_0=5.64$, black hole apparent horiozon we have $C_p/C_A=85$ and $C_p/C_e=19\times10^3$.

Another important quantity that can be obtained from the horizon is its mass

$$M_{\rm AH}^2 = \frac{A}{16\pi} + \frac{4\pi J^2}{A}, \tag{38}$$

and the related quantity, the maximum radiation loss (MRL),

$$\mathrm{MRL} = 1 - M_{\rm AH}/M_{\rm ADM}. \tag{39}$$

The MRL is the amount of energy that can be emitted if the black hole swallows none of the radiation energy present outside the horizon on the initial slice during its subsequent evolution.

We will also be interested in discussing what we call the ''transition points'' of the horizon. These are points in parameter space of the initial data problem at which the apparent horizon ceases to be on the throat (which is always a trapped surface) of the spacetime. The transition points can be accompanied by discontinuous changes in the character of the horizon, as measured by the quantities discussed here.

## IV. SURVEY OF INITIAL DATA SETS

We now apply a number of these horizon measures developed above to analyze a series of initial data sets, beginning with distorted, nonrotating holes.

### A. Time-symmetric Brill wave data

First we begin by examining the shape parameter, $C_p/C_A$, for a series of Brill wave plus black hole spacetimes. These nonrotating black holes provide a good starting point for our survey. Figure 2 shows $C_p/C_A$ for a set of black holes with $\sigma=1.5$, and the Brill wave amplitude, $Q_0$, in the range $-1<Q_0<7$.

The apparent horizon generally becomes prolate if it is distorted with a positive amplitude Brill wave, and oblate if it is distorted by a negative amplitude Brill wave [10]. However, the shape of the horizon undergoes two sharp transitions, one at about $Q_0=-0.65$ [10] and the other at about $Q_0=4.5$. Between these two values of $Q_0$ the horizon is on the throat, and the ratio $C_p/C_A$ grows exponentially. The further we move outside this region the further out the apparent horizon moves, and the more spherical the black hole becomes.

The spacetime behaves as if increasing amounts of energy were being deposited in the region somewhat away from the horizon as $|Q_0|$ is increased. Beyond a certain critical threshold, one would expect a new horizon would be formed. Beyond this range, the spacetime is still becoming more distorted, but the distortion is driving the apparent horizon further out on the grid and as a result the distortion is now primarily interior to the apparent horizon. Thus the exterior region becomes more spherical as this parameter is increased (see also Beig and Ó Murchadha [42] for understanding this effect).

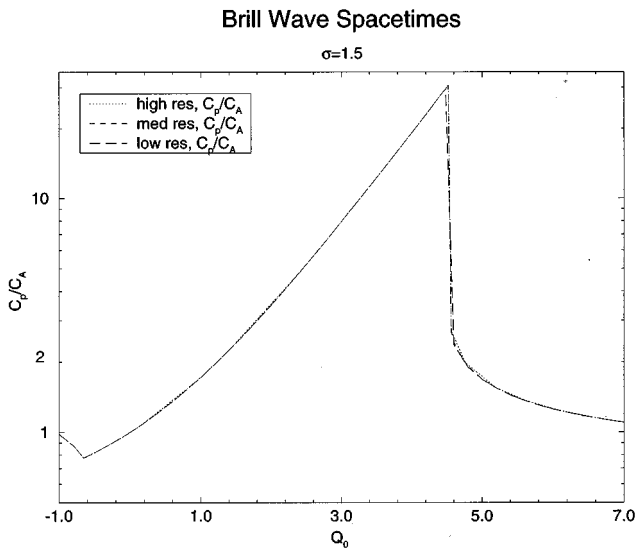


FIG. 2. We plot the apparent horizon shape parameter $C_p/C_A$, where $C_p$ and $C_A$ are the polar and ''areal'' circumferences of the surface, for a set of nonrotating distorted black hole initial data sets. The shape parameter is plotted against $Q_0$, the amplitude of the distorting Brill wave. All spacetimes shown here have the same Brill wave width, $\sigma=1.5$, the width that best characterizes the geometry of the Kerr spacetime. This plot shows the same data as computed on three grids with increasingly more zones, which illustrates how close we are to the exact solution. These results are second-order convergent.

Next we show the effect of changing the width of the Brill wave. In Fig. 3 we show a set of spacetimes like those shown above, but a larger width Brill wave is used ($\sigma=3.5$). We see that the horizon stays on the throat for larger values of $Q_0$, thereby making the maximum distortion parameter much larger. This results in a value of $C_p/C_A$ that is about an order of magnitude larger than the $\sigma=1.5$ distortion. The lower transition is still at about $Q_0=-0.65$, but now the upper transition has moved to $Q_0=5.65$. The decrease in $C_p/C_A$ as we move away to values of $Q_0$ larger than 5.65 also becomes less sudden.

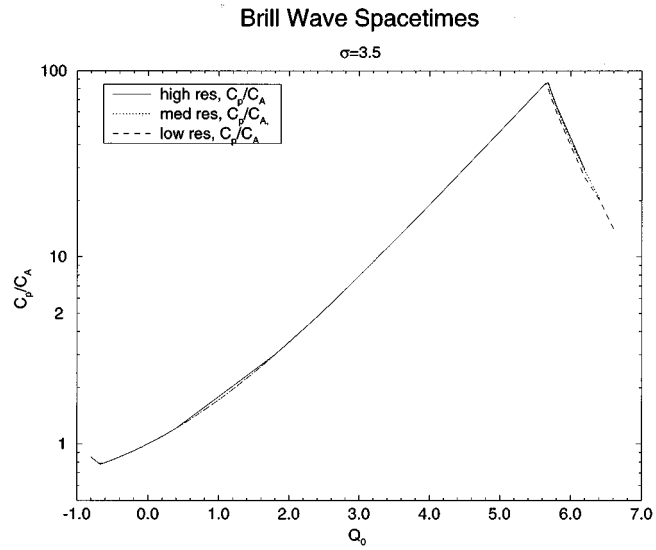


FIG. 3. This plot illustrates the basic properties of the apparent horizon shape parameter, $C_p/C_A$, for the large width Brill wave, $\sigma=3.5$. The apparent horizon becomes extremely distorted near $Q_0=5.65$, with $C_p/C_A\approx 90$. This plot shows the same data as computed on three grids with increasingly more zones.

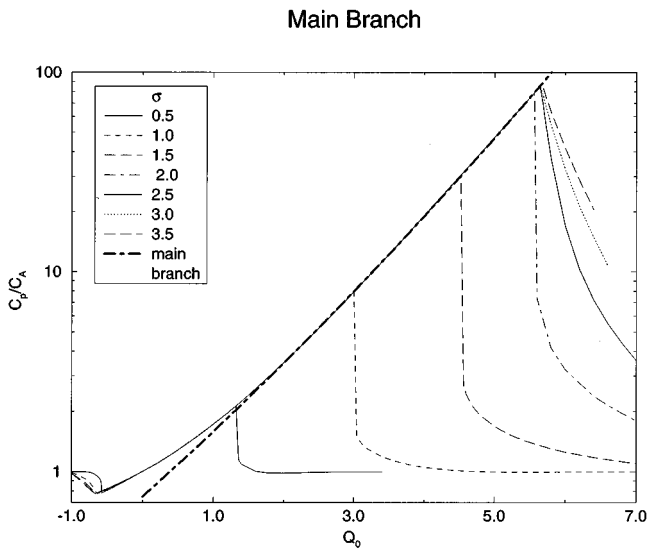


FIG. 4. We illustrate the prolateness (large $C_p/C_A$) of the apparent horizon for spacetimes with Brill wave distortions of varying amplitude, $Q_0$, and a variety of widths, $\sigma$. Also plotted is a fit of the ''main branch,'' a curve on which horizons lie for all distorted black hole spacetimes considered. For each family we consider, there is a transition point, a critical amplitude above which the horizon jumps off the throat and becomes more spherical.

In Fig. 4 we now show the data from the previous two graphs along with a number of spacetimes with varying Brill wave widths, $\sigma$. The values of $\sigma$ considered are 0.5, 1.0, 1.5, 2.0, 2.5, 3.0, and 3.5. We will call this group of spacetimes *set 1a*. We see that the function $C_p/C_A$ of $Q_0$ changes only slightly as $\sigma$ is varied for a large portion of the plot. There is a sharp transition that occurs for positive amplitude distortions which is strongly dependent on the width of the wave. Beyond this transition point the AH ceases to be on the throat. There is another transition point for the negative amplitude Brill wave spacetimes, and for all but the narrowest of the Brill waves considered ($\sigma=0.5$) it lies at about $Q_0=-0.65$. The region between these two transitions constitutes what we will call the ''main branch'' and is relatively independent of $\sigma$. The ''main branch'' for the range $1.8<Q_0<5.6$ is approximated to an accuracy of 1% or less by

$$C_p/C_A=\exp(-0.287055+0.728645Q_0+0.019728Q_0^2), \tag{40}$$

and is plotted by a heavy dashed line in Fig. 4. Since the horizon is simply the throat ($\eta=0$) for the ''main branch'' spacetimes it is not surprising that $\log(C_p/C_A)$ should depend linearly on $Q_0$ as it is simply reflecting the effect of $Q_0$ upon the conformal metric.

Also worthy of note is that above $\sigma=2.0$ the upper transition point becomes nearly fixed at $Q_0=5.65$. Some small

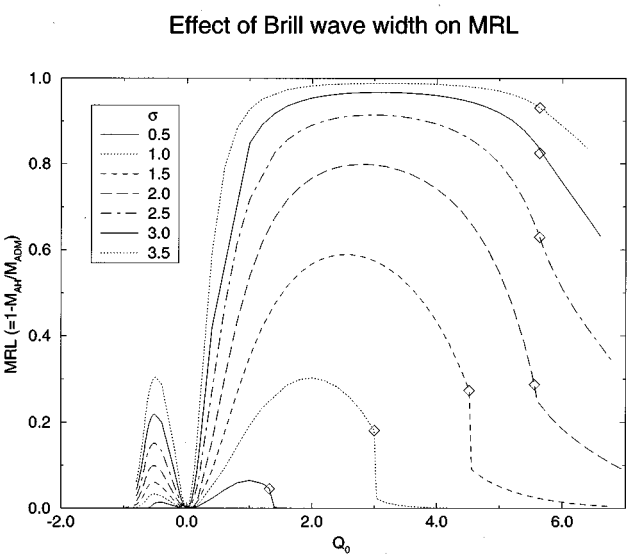


FIG. 5. This plot illustrates the maximum radiation loss, or MRL, for spacetimes with Brill wave distortions of varying amplitude, $Q_0$, and a variety of widths, $\sigma$. The diamonds mark the location of the maximally prolate horizon for each curve.

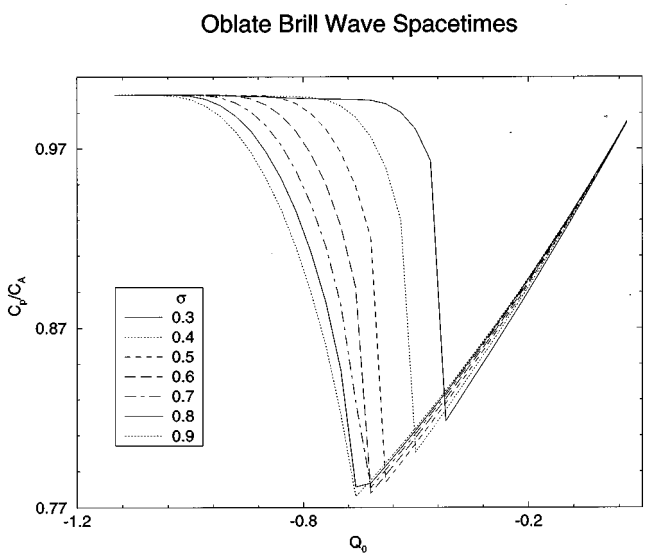


FIG. 6. This plot illustrates the behavior of the negative amplitude, narrower width Brill wave spacetimes. The behavior here is qualitatively similar to the larger width positive amplitude spacetimes depicted in Fig. 4, except that the apparent horizons are all oblate. As $Q_0$ becomes more negative the apparent horizon jumps off the throat at a transition point and the spacetime becomes more spherical.

variation occurs, but not much. Roughly $\sigma=2$ is a width above which the most prolate spacetime occurs at about $Q_0=5.6$ with a shape characterized by $C_p/C_A\approx 88$. Likewise, it appears that $\sigma=1$ is a width above which the most oblate spacetime occurs at about $Q_0=-0.65$ with a shape characterized by $C_p/C_A\approx 0.77$.

In Fig. 5 we see the effect of $Q_0$ and $\sigma$ on the MRL of the spacetime for *set 1a*. For reference we have marked the positive $Q_0$ transition points, the peaks in the plot of $C_p/C_A$ that are seen in Fig. 4, with diamonds in Fig. 5. The MRL increases, in all cases, as we increase $|Q_0|$ until it reaches some maximum value. As we increase $|Q_0|$ further, we arrive at a transition point. Along the path of increasing $|Q_0|$, the energy of the spacetime first increases primarily because we are adding wave energy outside the horizon. As we travel further in this parameter space the mass increases primarily because energy is being added to the hole itself. Another feature that can be observed in Fig. 5 is that the MRL of the transition point begins to rise much more rapidly with increasing $Q_0$ after the Brill wave width becomes greater than 2.

In both Figs. 2 and 3 we have plotted the curves for Brill waves with widths $\sigma=1.5$ and $\sigma=3.5$ respectively at three different grid resolutions: $600\times 96$, $300\times 48$, and $150\times 24$. We note that in both cases the resolution lines are very close together and that the convergence exponent $\xi$, as defined by

$$\left(\frac{C_p}{C_A}\right)_{\text{num}}-\left(\frac{C_p}{C_A}\right)_{\text{true}}\propto(\Delta\eta)^{\xi}+\cdots, \tag{41}$$

is very nearly 2 at all points on both graphs. The larger width Brill waves were more difficult to calculate, but our code is capable of calculating these spacetimes accurately.

### B. Negative amplitude Brill wave distortions

In this section we focus on the region of the time-symmetric distorted black hole spacetime in which the amplitude of the distortion is negative. In this regime we find a behavior that is qualitatively similar to the behavior seen for positive amplitude distortions in *set 1a*, but we found that we needed to use narrower Brill waves to explore this effect for negative amplitude spacetimes. If we consider Fig. 4 we see that all but the $\sigma=0.5$ curves are very similar for the negative amplitude portion of the graph. Because of this we use widths $\sigma=0.3$, 0.4, 0.5, . . . ,0.9 and we plot this data in Fig. 6. We label this data as *set 1b*.

Note in Fig. 6 that the maximum distortion (minimum $C_p/C_A$) is increased by widening the Brill wave until a limiting value is reached, a behavior similar to that observed for positive amplitudes in Fig. 4. There is also a continuation of the main branch for the segment of the spacetimes in which the wave is on the throat, although we have not computed a fit in this case.

### C. Brill wave distortions of Bowen and York rotating black holes

In this section we discuss spacetimes with $\sigma=1.5$, $-1<Q_0<7$ and angular momentum parameter $J=0.25$, $J=0.5$, and $J=5$, and we will call this collection *set 2a*. We plot $C_p/C_A$ for this set in Fig. 7. One can see from the figure that the rotating black holes still lie along the main branch, but the transition points occur earlier (for smaller $Q_0$).

Adding angular momentum to Brill wave spacetimes reduces the value of $C_p/C_A$, thereby making the spacetime more oblate. For the larger amplitude Brill waves this effect is quite marked. In Fig. 8 we make this point clearer by graphically depicting the embeddings of several distorted black hole spacetimes. Three Brill wave spacetimes are taken as starting points: $Q_0=-0.1$, 0.0, and 0.1, and are plotted with thick lines. Next to each of these lines is a thinner one

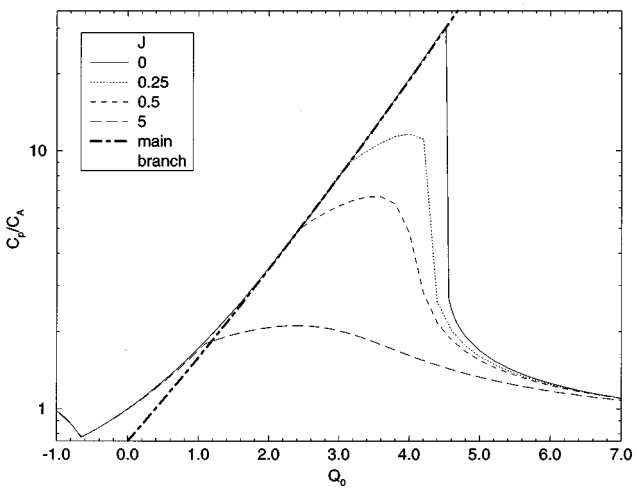


FIG. 7. This figure illustrates the effect on the apparent horizon of a Brill wave distortion on a Bowen and York black hole. The addition of angular momentum makes the transition point, the point where the horizon leaves the throat, occur sooner, although for small values of $Q_0$ the value of $C_p/C_A$ is very close to the ''main branch.''

depicting the shape of the horizon after setting $J=10$. This general trend, that angular momentum makes a horizon more oblate was a feature that was observed previously by Smarr for the Kerr spacetime [36].

As mentioned above, one generally expects that rotating black holes will be potentially more oblate than nonrotating spacetimes. However, there is an exception to this. In Fig. 9 we extend the above plots to show in more detail the effect of rotation on the negative amplitude spacetimes. We see data sets which cover input parameters in the range $-0.657<Q_0<-0.655$, with $\sigma=1.5$ and $0<J<10$ (*set 2b*). Thus, while the addition of angular momentum to a spacetime usually makes an AH more oblate, this is not always true. In fact, the addition of the Bowen and York distortion makes the minimum $C_p/C_A$ as a function of $Q_0$ *larger*. In other words, while adding a negative amplitude Brill wave to a given black hole *can* make it more oblate, increasing $J$ also makes the horizon jump off the throat at a smaller value of $|Q_0|$ so that it does not achieve the maximum oblateness seen with no rotation.

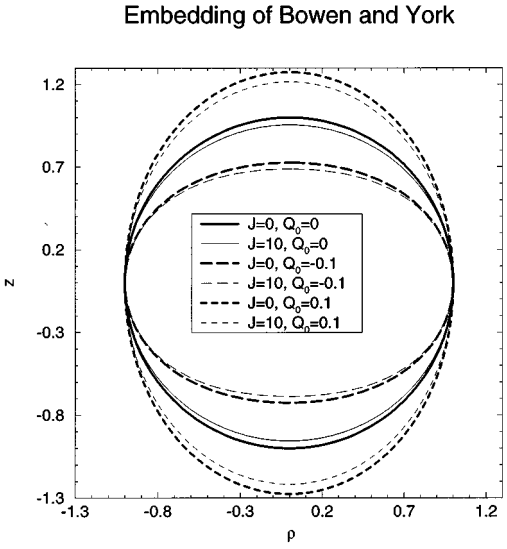


FIG. 8. In this plot we see the embeddings of several distorted black hole spacetimes. The heavy lines are spacetimes distorted by Brill waves: a prolate spacetime with $Q_0=0.1$, an oblate spacetime with $Q_0=-0.1$, and a Schwarzschild spacetime with $Q_0=0.0$. The lighter lines represent these same spacetimes with angular momentum added.

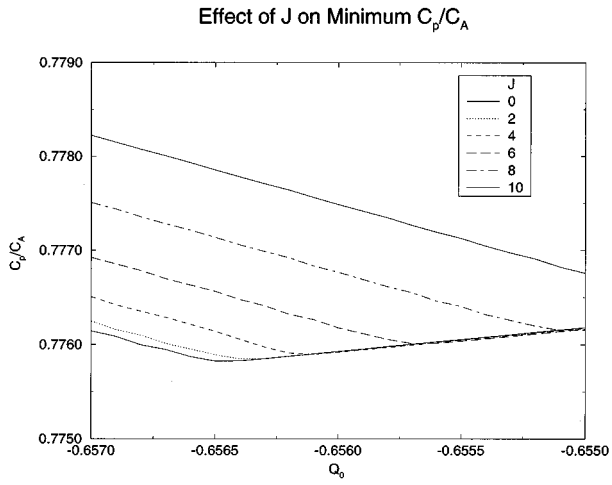


FIG. 9. In this plot we see data sets which cover input parameters in the range $-0.657<Q_0<-0.655$, with $\sigma=1.5$ and $0<J<10$ (*set 2b*). It illustrates that although $J$ usually makes a horizon more oblate, it can also cause the horizon to leave the throat for sufficiently negative values of $Q_0$ and thereby make it more spherical rather than more oblate.

Although we do not provide a plot, we note that as the parameter $J$ is increased for these spacetimes, the MRL decreases.

### D. Brill wave distortions of end-stage ''cosmic screws''

We next examine a collection of ''cosmic screw'' spacetimes, referred to as *set 3*. The data in *set 3* is identical to the data in *set 2a* (distorted Bowen and York black holes) with the exception that it uses the cosmic screw form of the perturbation. The value of $J_{\rm screw}$ clearly creates a much smaller distortion of the horizon than the Bowen and York angular momentum parameter of the same value, as is evident in Fig. 10. Indeed, it is almost impossible to distinguish the $J_{\rm screw}=0.5, 0.25$ spacetimes. This is reasonable since this distortion can be thought of as two counterrotating and therefore counteracting Bowen and York distortions.

### E. Odd-parity distortions of Schwarzschild

In this section we examine *set 4*, which comprises odd-parity distortions of the form $f_1=0$, $f_2=q'_G$, and $f_3=\cos\theta$ [see Eq. (24)], with parameters $\eta_0=0$, $0<Q_0<100$, $\sigma=0.5$, 1.5, 2.0, 2.5, 3.0, and 3.5.

This family of spacetimes, depicted in Fig. 11, displays the same property of the pure Bowen and York data distortions (in which $J$, the angular momentum parameter, can be thought of as representing the amplitude of the extrinsic curvature distortion), namely that there is no limit to the magnitude of the parameter $J$ that is possible, either theoretically or in any numerical test done to date. We do not feature the

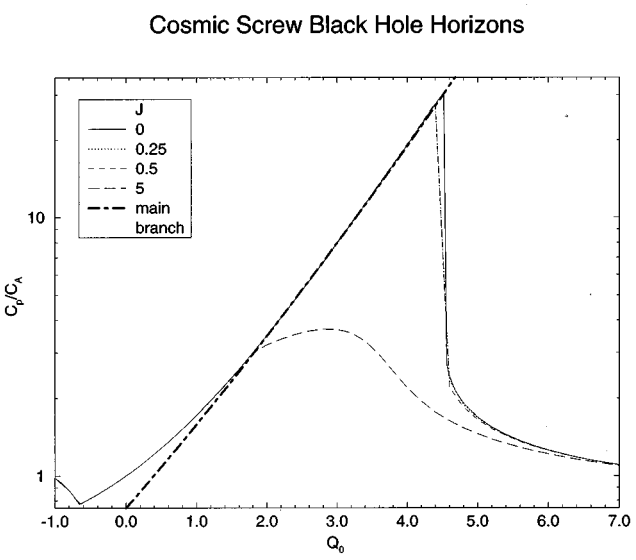


FIG. 10. This figure illustrates the effect on the apparent horizon of a Brill wave distortion on a black hole with a ''cosmic screw'' distortion (counterrotating above and below the equatorial plane but without net angular momentum, see text for details). As in the case of the Bowen and York black holes, the boundary conditions the cosmic screw have is the effect of smoothing out the $C_p/C_A$ curve, although it has a lesser effect than a Bowen and York distortion with the a distortion parameter of equal value.

negative amplitude distortions of these sets because the relevant terms are squared in the Hamiltonian constraint, making their overall sign unimportant.

Unlike the Bowen and York spacetime, for which the horizon remains on the throat for very large $J$, the horizon moves away from the throat in the odd-parity distortion of Schwarzschild for sufficiently large $Q_0$. In this respect these data sets are similar to *set 1a*. They also resemble *set 1a* in that larger width distortions make it possible to achieve more distorted horizons. *Set 4* is unlike *set 1a* in that the distortion never becomes even remotely as large (note that this distortion is in the extrinsic curvature and affects the three-metric only through the conformal factor, it is not the standard Brill wave distortion).

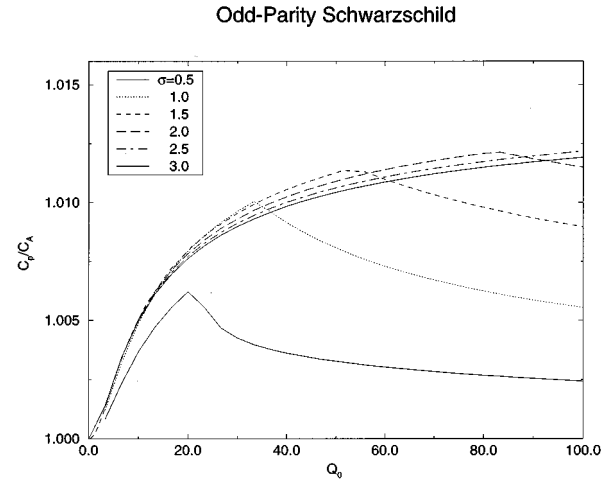


FIG. 11. This plot shows the prolateness of the horizon, $C_p/C_A$, for a odd-parity data sets with a variety of distortion widths $\sigma$. As was the case for the Brill wave distorted spacetimes (compare to Fig. 4 above), the maximum in the $C_p/C_A$ curve marks the place where the apparent horizon moves away from the throat.

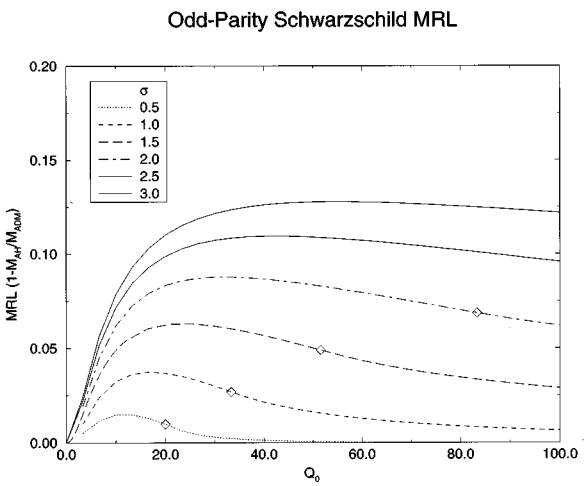


FIG. 12. This plot shows the MRL for a variety of odd-parity data sets. Qualitatively it has the same features observed in Fig. 5, except that the magnitude of the MRL is much smaller. As in Fig. 5, diamonds mark the amplitudes at which a given black hole spacetime has its maximum value of $C_p/C_A$.

Figure 12 shows the behavior of the MRL function for *set 5*. As in *set 1a* this data set has its peak MRL somewhat before the horizon departs from the throat. It is otherwise qualitatively similar to the MRL curves depicted in Fig. 5.

### F. Hoop conjecture

An important question that we wish to discuss is ''How distorted can a black hole be?'' The hoop conjecture [11,12] states that an event horizon will form if and only if the matter is sufficiently compact in all directions. This conjecture would seem to suggest that the black hole horizon should also be sufficiently compact in all directions. Although interesting work has been done on the hoop conjecture for black hole spacetimes (see, e.g [37,38]) much remains to be done.

As we have seen above, black hole *apparent* horizons can be extremely distorted, nonspherical objects as measured by the shape parameter $C_p/C_A$. We have shown cases where the AH is extremely prolate ($C_p/C_A \approx 88$) or oblate ($C_p/C_A \approx 0.77$). However, these results are for the apparent horizon, and not the *event* horizon. A careful study of distorted event horizons, and implications on the hoop conjecture will be presented elsewhere. In this section we restrict our attention to the apparent horizons we have found, and discuss whether there is a limit to how distorted they can be.

The fact that there are limits on the amplitude parameter ($Q_0$) is somewhat suggestive of a limit on the degree of distortion possible for the apparent/event horizon of the black holes considered here (since the amplitude parameter controls the degree of distortion of the black hole). Indeed, it allows one to demonstrate the limit numerically for a Brill wave of a given shape (as given by $\sigma$, $\eta_0$, and $n$).

However, there may also be a good reason to suppose that there is no limit on how large or small the quantity $C_p/C_A$ may become for an asymptotically flat spacetime. We might be able to engineer spacetimes with two gravity wave distor-

tions: one widely extended, the other more comparable to the size of the hole. In effect, the larger distortion can be used to ''fool'' the black hole into thinking that the spacetime is not asymptotically flat. Thus, it may be that we can find spacetimes with arbitrarily large $C_p/C_A$ if we combine distortions on a variety of scales. This possibility is not investigated here.

### G. Maximum prolateness

It is difficult to pin down a maximum prolateness for all the types of spacetimes considered here. It seems reasonable, however, to simply focus on Brill wave spacetimes since the odd-parity and momentum distortions usually make the spacetime more oblate or have small effect. For any given value of $\sigma$ it is a straightforward matter to obtain the value of $Q_0$ which maximizes $C_p/C_A$ because we can search the entire range of possible values for $Q_0$ (which we know from Sec. II C must have a value less than 10.0).

In all these data sets, the horizon remains on the throat until some critical value of $Q_0$ is reached and then it departs and moves outward in coordinate space. Until the horizon leaves the throat, $C_p/C_A$ continues to grow, but as soon as it departs this ratio begins to decrease. This downward trend in $C_p/C_A$ continues as $Q_0$ is increased until a value of $Q_0$ is reached which is inconsistent with asymptotic flatness. The most distorted spacetime occurs when the largest value of $\sigma$ is used, although the growth is very slow after the value of $\exp(\sigma)$ has increased to about half the fundamental $\ell=2$ wavelength of the black hole.

While the information we obtained does not provide us with a definite answer about the maximum possible prolateness of the apparent horizon in these spacetimes, it suggests that there is some limiting value of $C_p/C_A$. The largest value we have measured is $C_p/C_A=88$. However, it is possible that despite the observed trends the quantity $C_p/C_A$ may be made to grow without limit for some untried Brill wave shape or combination of shapes.

### H. Maximum oblateness

How oblate can a black hole be? To get a feel for the meaning of the ratio $C_p/C_A$ we note that for an infinitely thin disk in Euclidean space we have $C_p/C_A=0.900$ and for an extremal Kerr black hole $(a/m=1)$ we have a smaller value, $C_p/C_A=0.860$. Thus, although these ratios are quite close to unity, they actually represent extremely distorted surfaces. For a very wide range of Brill wave parameters we have seen a robust lower bound for $C_p/C_A\approx 0.77$, with $Q_0=-0.65$, as discussed above. This seems to follow the trend discussed above for the prolate black hole spacetimes.

### I. Penrose inequality

In 1973 Penrose proposed a criterion for a spacetime which, if violated, would indicate cosmic censorship would be violated [39]. The criteria is simply that the irreducible apparent horizon mass must be less than or equal to the ADM mass.

Jang and Wald proved [40] the inequality for spacetimes with a single AH of topology $S^2$ which also satisfies a certain mathematical condition. (It essentially states that it is possible to foliate the region of the spacetime exterior to the apparent horizon with a sequence of nested two-surfaces, which are asymptotically spheres at large radii, using a ''lapse'' whose value is equal to the inverse of the extrinsic curvature of those two-surfaces.) We have not shown that this condition is actually satisfied for the wide class of black hole spacetimes considered here, but we have seen that this inequality is preserved in all spacetimes considered in this paper. Bernstein also sought for and failed to find a violation of the Penrose inequality [10,17] using the Brill wave distortions of the non-rotating black hole, but did not consider the extreme distortions used in this paper. A violation of the Penrose inequality would result in a negative value for the MRL, and we can see that this does not occur if we review Figs. 5 and 12.

## V. SUMMARY AND FUTURE WORK

In this paper we have described the construction of new initial data sets for distorted rotating black holes in detail. These data sets correspond to a large family of black hole spacetimes, generalizing the Kerr [18], Bowen and York [19], distorted Schwarzschild black holes [17], and should provide a rich testing ground for evolutions of highly dynamic, rotating and nonrotating black holes.

We have analyzed many of the properties of extreme parameter choices of these data sets. We have, for example, located the analytic upper and lower limits to the possible distortion parameters for these spacetimes, located the transition points beyond which multiple trapped surfaces exist, and identified spacetimes with the most oblate/prolate apparent horizons in our family of data sets. Furthermore, we investigated the effect of rotation and cosmic-screw type distortions on these data sets. This investigation should help provide a roadmap to interesting, distorted black hole spacetimes for evolution in both 2D and 3D.

In the near future we intend to apply the horizon finding code described in Ref. [41] to some of the above data sets, to determine to what extent the behavior of the event horizons is in agreement with the behavior of the more extremely distorted apparent horizons. Do spacetimes with strongly distorted apparent horizons have strongly distorted event horizons? This research provides us with important data for this investigation. In particular, $\sigma=2$ configurations with amplitudes $Q_0>3.5$ seem likely to yield the most distorted spacetimes. We also plan to evolve the cosmic screw spacetimes and study them in more detail.

## ACKNOWLEDGMENTS

We would like to thank Pete Anninos, David Bernstein, Karan Camarda, Greg Cook, Paul Walker, Larry Smarr, and especially Wai-Mo Suen for many helpful suggestions throughout the course of this work. This work was supported by NCSA, NSF grants PHY94-07882 and ASC/PHY93-18152 (ARPA supplemented). The numerical calculations were performed at NCSA on the SGI Power Challenge and at the Pittsburgh Supercomputing Center on the Cray C-90. Some symbolic calculations were performed using MATHEMATICA and MATHTENSOR.

[1] A. A. Abramovici *et al.*, Science **256**, 325 (1992).
[2] K. Thorne, in *Proceedings of the Eight Nishinomiya-Yukawa Symposium on Relativistic Cosmology*, edited by M. Sasaki (Universal Academy Press, Tokyo, Japan, 1994).
[3] A. Abrahams, D. Bernstein, D. Hobill, E. Seidel, and L. Smarr, Phys. Rev. D **45**, 3544 (1992).
[4] P. Anninos, D. Bernstein, D. Hobill, E. Seidel, L. Smarr, and J. Towns, in *Computational Astrophysics: Gas Dynamics and Particle Methods*, edited by W. Benz, J. Barnes, E. Muller, and M. Norman (Springer-Verlag, New York, 1994).
[5] P. Anninos, D. Hobill, E. Seidel, L. Smarr, and W.-M. Suen, Phys. Rev. Lett. **71**, 2851 (1993).
[6] P. Anninos, D. Hobill, E. Seidel, L. Smarr, and W.-M. Suen, Phys. Rev. D **52**, 2044 (1995).
[7] P. Anninos, D. Bernstein, S. Brandt, J. Libson, J. Massó, E. Seidel, L. Smarr, W.-M. Suen, and P. Walker, Phys. Rev. Lett. **74**, 630 (1995).
[8] R. Matzner, E. Seidel, S. Shapiro, L. Smarr, W.-M. Suen, S. Teukolsky, and J. Winicour, Science **270**, 941 (1995).
[9] P. Anninos, K. Camarda, J. Massó, E. Seidel, W.-M. Suen, and J. Towns, Phys. Rev. D **52**, 2059 (1995).
[10] D. Bernstein, Ph.D. thesis, University of Illinois Urbana-Champaign, 1993.
[11] K. Thorne, in *Magic Without Magic: John Archibald Wheeler*, edited by J. Klauder (Freeman, San Francisco, 1972), p. 231.
[12] C. W. Misner, K. S. Thorne, and J. A. Wheeler, *Gravitation* (Freeman, San Francisco, 1973), p. 867.
[13] A. Einstein and N. Rosen, Phys. Rev. **48**, 73 (1935).
[14] C. Misner, Phys. Rev. **118**, 1110 (1960).
[15] D. S. Brill and R. W. Lindquist, Phys. Rev. **131**, 471 (1963).
[16] D. S. Brill, Ann. Phys. (N.Y.) **7**, 466 (1959).
[17] D. Bernstein, D. Hobill, E. Seidel, and L. Smarr, Phys. Rev. D **50**, 3760 (1994).
[18] R. P. Kerr, Phys. Rev. Lett. **11**, 237 (1963).
[19] J. Bowen and J. W. York, Phys. Rev. D **21**, 2047 (1980).
[20] G. Cook, Ph.D. thesis, University of North Carolina at Chapel Hill, Chapel Hill, North Carolina, 1990.
[21] G. B. Cook, Phys. Rev. D **50**, 5025 (1994).
[22] S. Brandt and E. Seidel, Phys. Rev. D **52**, 856 (1995).
[23] S. Brandt and E. Seidel, Phys. Rev. D **52**, 870 (1995).
[24] S. Brandt and E. Seidel, in *General Relativity*, Proceedings of the 7th Marcel Grossmann Meeting on General Relativity, Stanford, California, 1994, edited by R. Ruffini and M. Keiser (World Scientific, Singapore, 1995).
[25] P. Anninos, D. Bernstein, S. Brandt, D. Hobill, E. Seidel, and L. Smarr, Phys. Rev. D **50**, 3801 (1994).
[26] C. W. Misner, K. S. Thorne, and J. A. Wheeler, *Gravitation* (Freeman, San Francisco, 1973).
[27] D. Bernstein, D. Hobill, E. Seidel, L. Smarr, and J. Towns, Phys. Rev. D **50**, 5000 (1994).
[28] C. Evans, in *Dynamical Spacetimes and Numerical Relativity*, edited by J. Centrella (Cambridge University Press, Cambridge, England, 1986), pp. 3–39.
[29] D. Bernstein and K. P. Tod, Phys. Rev. D **49**, 2808 (1994).
[30] D. Bernstein, D. Hobill, and L. Smarr, in *Frontiers in Numerical Relativity*, edited by C. Evans, L. Finn, and D. Hobill (Cambridge University Press, Cambridge, England, 1989), pp. 57–73.
[31] N. Ó Murchadha and J. York, Phys. Rev. D **10**, 2345 (1974).
[32] T. Regge and J. Wheeler, Phys. Rev. **108**, 1063 (1957).
[33] M. Cantor and D. Brill, Compositio. Mathematica. **43**, 317 (1981); we thank Robert Bartnik for pointing out this reference to us.
[34] M. W. Choptuik and W. G. Unruh, Gen. Relativ. Gravit. **18**, 818 (1986).
[35] G. Gibbons, Commun. Math. Phys. **27**, 87 (1972).
[36] L. L. Smarr, Phys. Rev. D **7**, 289 (1973).
[37] E. Flannagan, Phys. Rev. D **44**, 2409 (1991).
[38] E. Flannagan, Phys. Rev. D **46**, 1429 (1992).
[39] R. Penrose, Ann. (N.Y.) Acad. Sci. **224**, 125 (1973).
[40] P. Jang and R. M. Wald, J. Math. Phys. **18**, 41 (1977).
[41] J. Libson, J. Massó, E. Seidel, W.-M. Suen, and P. Walker, Phys. Rev. D **53**, 4335 (1996).
[42] R. Beig and N. Ó Murchadha, Phys. Rev. Lett. **66**, 2421 (1991).